CHEMISTRY OF MATERIALS

pubs.acs.org/cm

Article

Stabilization of Cu_2O through Site-Selective Formation of a Co_1Cu Hybrid Single-Atom Catalyst

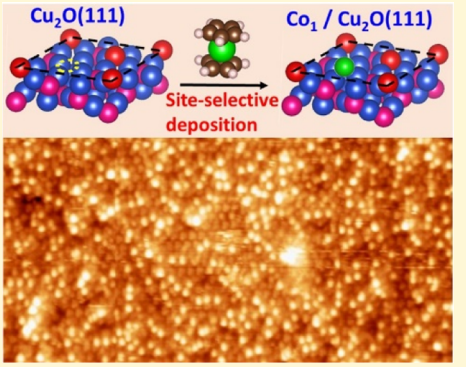
Chunlei Wang,[○] Yuan Kong,[○] Markus Soldemo, Zongfang Wu, Héloise Tissot, Burcu Karagoz, Kess Marks, Joakim Halldin Stenlid, Andrey Shavorskiy, Esko Kokkonen, Sarp Kaya, Dario J. Stacchiola, and Jonas Weissenrieder*

Cite This: *Chem. Mater.* 2022, 34, 2313−2320

Read Online

ACCESS | Metrics & More | Article Recommendations | Supporting Information

ABSTRACT: Single-atom catalysts (SACs) consist of a low coverage of isolated metal atoms dispersed on a metal substrate, called single-atom alloys (SAAs), or alternatively single metal atoms coordinated to oxygen atoms on an oxide support. We present the synthesis of a new type of Co_1Cu SAC centers on a $Cu_2O(111)$ support by means of a site-selective atomic layer deposition technique. Isolated metallic Co atoms selectively coordinate to the native oxygen vacancy sites (Cu sites) of the reconstructed $Cu_2O(111)$ surface, forming a Co_1Cu SAA with no direct Co−O_x bonds. The centers, here referred to as Co_1Cu hybrid SACs, are found to stabilize the active Cu^+ sites of the low-cost Cu_2O catalyst that otherwise is prone to deactivation under reaction conditions. The stability of the $Cu_2O(111)$ surface was investigated by synchrotron radiation-based ambient-pressure X-ray photoelectron spectroscopy under reducing CO environment. The structure and reduction reaction are modeled by density functional theory calculations, in good agreement with experimental results.



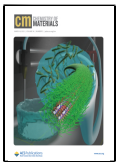
Downloaded via KOC UNIV on November 3, 2022 at 14:07:12 (UTC).
See https://pubs.acs.org/sharingguidelines for options on how to legitimately share published articles.

INTRODUCTION

Copper-based catalysts have attracted extensive attention as future replacement of noble metal catalysts due to abundant copper reserves and their promising application in several heterogeneous catalytic reactions.[1−9] Cu_2O catalysts have been successfully deployed in reactions of CO oxidation,[1,2] N_2O activation,[3] propylene epoxidation,[4,5] water−gas shift reaction,[6] photocatalytic water splitting,[7] methanol synthesis,[8] and CO_2 reduction.[9] However, deactivation is a persistent problem for copper-based catalysts. Deactivation often proceeds through complete oxidation to copper(II) oxide or reduction to metallic copper nanoparticles, both results in the loss of active Cu^+ sites.[5,10−15] Insufficient stability has hindered further development of industrial applications and thus needs to be addressed.

Single-atom catalysts (SACs) have recently become a topic at the forefront of catalytic research, in particular due to their excellent catalytic properties combined with a maximized utilization of metal.[16] The SAC concept was proposed in the synthesis of single-atom Pt on a metal-oxide support and have since been followed by a series of powder single-atom catalyst studies.[17,18] However, a fundamental description of the catalytic mechanisms underpinning the properties of SAC remains elusive, mainly because of the material complexity of applied catalysts and limitations of current experimental techniques.[16,19] Model studies of SACs, realized by deposition of atomically dispersed metal atoms on well-defined single crystals, have been fervently deployed to investigate and predict structure-function relationships.[20−23] Traditional physical vapor deposition (PVD) methods are frequently used in the metal deposition process.[24] The model systems are often studied with surface-sensitive techniques, such as X-ray photoelectron spectroscopy (XPS) or scanning tunneling microscopy (STM), that allow extraction of catalytic information at an atomic level. An emerging branch of SACs, which was first proposed in surface science model studies, is single-atom alloys (SAAs).[25,26] Preparation of SAAs systems generally proceeds through deposition of a low coverage of metal atoms on a single crystalline metal support. The adsorbed metal atoms remain isolated through strong metal−support interactions.[27,28] Owing to their unique electronic and geometric structures, SAA catalysts have demonstrated superior catalytic properties for many reactions, including selective hydrogenation, methanol reforming, and resistance to deactivation via coke formation.[20,29−31] However, is it possible to synthesize a single-atom alloy directly on a metal-oxide support with similar qualities as on a metal support?

Received: December 2, 2021
Revised: January 19, 2022
Published: February 3, 2022



ACS Publications

© 2022 The Authors. Published by American Chemical Society

https://doi.org/10.1021/acs.chemmater.1c04137
Chem. Mater. 2022, 34, 2313−2320

Realization of such a system would bridge the gap between SAAs and traditional SACs and may provide a new venue for understanding heterogeneous catalysis.

In this paper, we use an atomic layer deposition (ALD) method, which is more suitable in scaled-up industrial applications than PVD methods, to selectively deposit the transition metal cobalt on oxygen vacancy sites of the reconstructed $Cu_2O(111)$-$(\sqrt{3} \times \sqrt{3})R30°$ surface. Selective deposition at vacancies allows for formation of an ordered surface at minimal occupancy, while maintaining high exposure of the desirable Cu^+ active catalytic centers. The ALD technique relies on precursor-governed self-limiting growth to synthesize new materials.[32] Isolated cobalt atoms with a density up to 0.29 ML (1 ML is here defined as one cobalt atom per $Cu_2O(111)$-$(\sqrt{3} \times \sqrt{3})R30°$ surface unit cell) were readily obtained by ALD growth, as confirmed by atomic resolution STM. The stability of the active Cu^+ sites was investigated in-situ using ambient-pressure XPS (APXPS) at reducing CO conditions. The APXPS results demonstrate a remarkable stabilization of the Cu^+ surface sites by the cobalt atoms. The cobalt bonding geometry was determined through density-functional theory (DFT) and XPS analysis, revealing a metallic state of the single cobalt atoms. The isolated cobalt atoms coordinate to surface copper sites and are not involved in direct bonding with the oxygen atoms of the substrate. The Co_1Cu center has the characters of SAAs but differs from traditional SAAs, where a metal is used as a support; therefore, we here label it as a Co_1Cu hybrid single-atom catalyst (HSAC).[20]

EXPERIMENTAL SECTION

STM Experiments. The $Cu_2O(111)$ surface was cleaned by cycles of sputtering (1×10^{-5} mbar Ar, 0.5 kV) and annealing in 1×10^{-6} mbar O_2 followed by a final annealing step in UHV. All the annealing steps were performed at 823−873 K for a duration of at least 10 min. The cleanliness and surface crystallinity of the $Cu_2O(111)$ single crystal was confirmed by STM and low energy electron diffraction (LEED), exhibiting a well-ordered $(\sqrt{3} \times \sqrt{3})R30°$ reconstruction. The STM study was carried out under UHV condition using an Omicron VT-STM operated in constant current imaging mode with electrochemically etched tungsten tips. The $Cu_2O(111)$ single crystal sample was purchased from the Surface Preparation Laboratory (the Netherlands).

After preparation of a clean sample, atomically dispersed cobalt atoms were selectively grown on the reconstructed $Cu_2O(111)$-$(\sqrt{3} \times \sqrt{3})R30°$ surface by ALD using cobaltocene ($CoCp_2$) and oxygen as precursors. The $CoCp_2$ powder (Acros Organics, 98%) was further purified by annealing at 373 K under vacuum for several hours to remove residual contaminants in the precursor. In the first half-cycle of the ALD process, the clean $Cu_2O(111)$ was exposed to $CoCp_2$ at room temperature with a precision leak valve. In the second half-cycle, the sample was exposed to 1×10^{-6} mbar O_2 at 473 K to remove the Cp ligands coordinated to cobalt. STM was conducted after the ALD growth. One monolayer (ML) is defined as one cobalt atom per $Cu_2O(111)$-$(\sqrt{3} \times \sqrt{3})R30°$ surface unit cell.

Ambient Pressure XPS. The APXPS experiments were conducted at the two APXPS endstations of the HIPPIE and the SPECIES beamlines at the MAX IV laboratory in Lund, Sweden.[33−35] The endstations have analysis chambers equipped with ambient pressure electron energy analyzers (Scienta-Omicron HiPP-3 and Specs PHOIBOS 150 NAP, respectively). After confirming the cleanliness of the sample by LEED and XPS, cobalt ALD synthesis was performed in the preparation chambers under conditions similar to the process established in the STM experiments. Subsequently, the sample was transferred to the ambient pressure cell for in-situ XPS studies at mbar pressures of reducing CO gas. The Co 2p, Cu 2p, and Cu LMM spectra were all collected at 1100 eV photon energy, and the O 1s spectra were collected at 750 eV. Fitting of XPS lines was performed by the Fit-XPS software (developed by David L. Adams, University of Århus, Denmark). The spectra were normalized to the background intensity on the low-binding energy side of the core level.

Computational Details. The DFT calculations were performed with the Vienna Ab-initio Simulation Package (VASP) version 5.4.[36−38] The Standard Projector-Augmented-Wave core-potentials, as well as the revised Perdew−Burke−Ernzerhof exchange−correlation functional, and a plane wave cutoff of 500 eV were used in the calculations.[39−41] All periodic slab calculations were carried out using a vacuum spacing of at least 14 Å. The $(\sqrt{3} \times \sqrt{3})$ slab contained six relaxed layers and three layers fixed to the Cu_2O bulk positions in total corresponding to three sandwiched Cu_2O layers. A $2 \times 2 \times 1$ Monkhorst−Pack k-point mesh was used. The surface model used in the calculations was based on previous structures of the $(\sqrt{3} \times \sqrt{3})R30°$ reconstruction of $Cu_2O(111)$ that also has been verified by LEED and atomic resolution STM analysis.[42−45] The characteristic $(\sqrt{3} \times \sqrt{3})R30°$ reconstruction of the $Cu_2O(111)$ surface was generated by removing one-third of the unsaturated surface oxygen atoms, corresponding to one oxygen vacancy per surface unit cell. A second type of surface reconstruction with both 1/3 ML oxygen vacancies and 1 ML monolayer copper vacancies was also considered. Spin-polarized calculations were conducted for all surfaces, and the convergence of the electronic energy and forces were set to 10^{-5} eV and 0.03 eV/Å, respectively. The transition states (TSs) were located by the climbing image nudged elastic band (CI-NEB) algorithm.[46] For the simulation of the density of states (DOS), the hybrid HF-DFT PBE0 functional was employed in the self-consistent field calculations.[47]

RESULTS AND DISCUSSION

The formation of the most stable $Cu_2O(111)$-$(\sqrt{3} \times \sqrt{3})R30°$ reconstructed surface was confirmed by STM and LEED, as shown in Figures 1b and S1. The results are in good agreement with our previous studies of the $Cu_2O(111)$ surface; further details are provided in the Supporting Information (Tables S1−S3).[42,45] The reconstruction of the $Cu_2O(111)$ surface is attributed to the removal of one-third of the under-coordinated surface oxygen atoms (Figure 1b, black dashed circle) with the formation of one oxygen vacancy per surface unit cell. The oxygen vacancy sites appear as protrusions in the STM images (e.g., Figure 1b).

ALD synthesis of the Co_1Cu HSAC was performed by alternately exposing the clean Cu_2O surface to precursors of $CoCp_2$ at 298 K and 1×10^{-6} mbar O_2 at 473 K, as illustrated in the schematic description in Figure 1a. Figure 1c shows a STM image of the $Cu_2O(111)$ surface after deposition of 0.059 ML $CoCp_2$ at 298 K. No clusters or nanoparticles were observed in the analysis. The protrusions, assigned to cobalt containing species, are located at the $Cu_2O(111)$ oxygen defect positions with an average apparent height of ∼0.27 nm (see Supporting Information Figure S2c). The results indicate dissociative adsorption resulting in formation of CoCp* species at oxygen vacancy sites (copper sites), as shown in the schematic model in Figure 1a. A dissociative adsorption mechanism is not surprising as it has been reported in other ALD studies using metallocenes.[48,49] The unsymmetrical shape of the protrusions is likely due to STM tip interactions with the Cp ligands of CoCp* species (see Figures 1c and S2a). The STM analysis also shows protrusions of lower apparent heights (Figure 1c, indicated by black arrows) than protrusions assigned to CoCp*. The lower protrusions are assigned to adsorbed Cp ligand fragments (Cp*) from the dissociative $CoCp_2$ adsorption process. The apparent height (∼0.14 nm)

https://doi.org/10.1021/acs.chemmater.1c04137
Chem. Mater. 2022, 34, 2313−2320

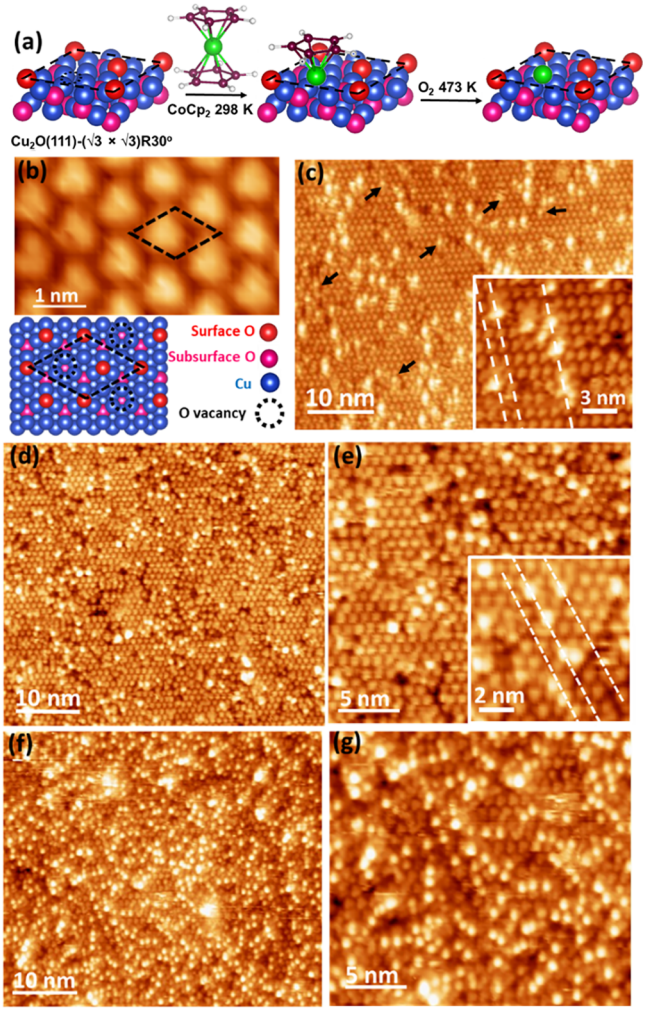


Figure 1. (a) Schematic illustration of ALD synthesis of Co_1Cu hybrid single-atom catalyst on a reconstructed $Cu_2O(111)$-$(\sqrt{3} \times \sqrt{3})R30°$ surface. (b) STM image of the clean Cu_2O surface (scanning parameters: −2.3 V, 0.12 nA) and its corresponding atomic structure model. The $(\sqrt{3} \times \sqrt{3})R30°$ unit cell is indicated by dashed black rhombuses. (c) STM images (−2.6 V, 0.14 nA) of the $Cu_2O(111)$ surface after adsorption of 0.059 ML $CoCp_2$ at 298 K and (d,e) STM images (−2.8 V, 0.16 nA) after annealing the surface shown in (c) under 1×10^{-6} mbar O_2 at 473 K. The dashed white lines in the insets of (c,e) serve as guides to the eye and are aligned along the oxygen vacancies of $Cu_2O(111)$. (f,g) STM images (−2.5 V, 0.14 nA) of $Cu_2O(111)$ after adsorption of 0.29 ML $CoCp_2$ at 298 K followed by annealing in 1×10^{-6} mbar O_2 at 473 K.

of the Cp* protrusions is close to what is expected from the geometrical height (~0.11 nm).[49]

After the following oxidation preparation step at 1×10^{-6} mbar O_2 and 473 K, the shapes of the Co containing protrusions become round and better defined (Figure 1d,e). The apparent height decreases from 0.27 to 0.21 nm (Figure S3c). Protrusions assigned to Cp* are no longer observed in the STM images, demonstrating their removal in the oxidation step. Annealing in 1×10^{-6} mbar O_2 at 473 K did not show a significant change in the coverage of protrusions assigned to Co-containing species (Figure 1c−e). The reduction in apparent height combined with more distinct STM imaging conditions indicates removal of the Co-coordinated Cp ligands. Figure 1f,g shows preparations with a higher density of protrusions (0.29 ML); additional STM images are shown in Figure S4. Registry analysis reveals that the Co-containing protrusions are predominantly located at the positions for the O vacancy site in the surface unit cell (inset to Figure 1e). The $Cu_2O(111)$ surface structure appears slightly distorted after cobalt deposition. The reconstruction may be tentatively attributed to a strong substrate interaction between cobalt and copper at the adsorption site.

Synchrotron radiation XPS was employed to determine the chemical state of the Co-containing species at the $Cu_2O(111)$ surface. Co 2p and O 1s spectra (Figure 2) were collected before and after an identical $CoCp_2$ exposure as in the STM studies in Figure 1f,g. Analysis of the O 1s from the clean $Cu_2O(111)$ surface shows two distinct components. The main peak is assigned to oxygen atoms residing at bulk lattice positions and the shoulder on the low binding energy side to surface oxygen atoms, as indicated in the atomic model in Figure 2d.[50,51] The Co $2p_{3/2}$ peak position was observed at a binding energy of 780.6 eV (Figure 2a). This is a shift of ~+1.3 eV compared to Co $2p_{3/2}$ for powder cobaltocene (779.3 eV),[52,53] suggesting a distinctly different interaction between the adsorbed CoCp* species and the Cu_2O support compared to Co−Cp bonds in cobaltocene. Careful inspection of the O 1s intensity shows a slight decrease following deposition (Figure 2b). This intensity decrease can be traced to adsorbate screening of the O 1s photoemission signal. The Co $2p_{3/2}$ peak shifts 1.0 eV towards lower binding energy (779.6 eV) after oxidation at 1×10^{-6} mbar O_2 and 473 K. The integrated intensity of the Co 2p remains the same, but a noticeable difference in the Co 2p line shape is observed (Figure 2a). The line shape after oxidation resembles metallic Co[54,55] and satellite features at ~786 eV or ~789 eV, characteristic for Co oxides, is absent from the spectrum.[55−57] An increase in the O 1s intensity at the expected position for a Co−O_x component (~529.5 eV) is also not observed (Figure 2c).[54,58] As such increase in O 1s intensity is not observed (blue dotted curve in Figure 2c), it can be concluded that CoO_x is not formed. In addition, C 1s analysis demonstrates the removal of Cp ligands from CoCp* species after annealing in O_2 (further details are provided in Figure S5 of the Supporting Information). Taken together, the Co $2p_{3/2}$ peak is assigned to metallic Co at a binding energy shift ~+1.1 eV with respect to metallic bulk Co (at ~778.5 eV).[54,59,60] Similar core-level shifts are not rare in transition metal alloys, for example, $AuCu_3$ results in Au 4f shifts of ~1 eV[61] and $Cu_{0.8}Pd_{0.2}$ in a Pd 3d shift of ~0.7 eV.[62] Co will donate charge to Cu in a CoCu alloy.[63] A similar ALD study of single-atom Co catalysts found no signs of Co−O_x bond formation even after treatment under oxidizing conditions.[64] Metal cluster size will also influence core level positions, as shown in a study by Wang et al. where a gradual increase in Pd 3d binding energy was observed as core−shell PdNi alloy islands and films were converted into atomically dispersed Pd.[65] The above shifts are similar to the shift observed for Co_1 in the present study and suggest formation of a Co_1Cu alloy. The STM and XPS results allow us to suggest the oxygen vacancies inherent to the $Cu_2O(111)$-$(\sqrt{3} \times \sqrt{3})R30°$ surface as adsorption sites in the formation of Co_1Cu HSAC.

DFT simulations were conducted to determine favorable adsorption sites and to describe bonding geometry at the experimentally investigated reaction steps of the ALD process. CoCp* and Co_1 were released at four locations in the unit cell: (a) under-coordinated oxygen site, (b) under-coordinated copper site, (c) oxygen vacancy site, and (d) copper site in the

https://doi.org/10.1021/acs.chemmater.1c04137
Chem. Mater. 2022, 34, 2313−2320

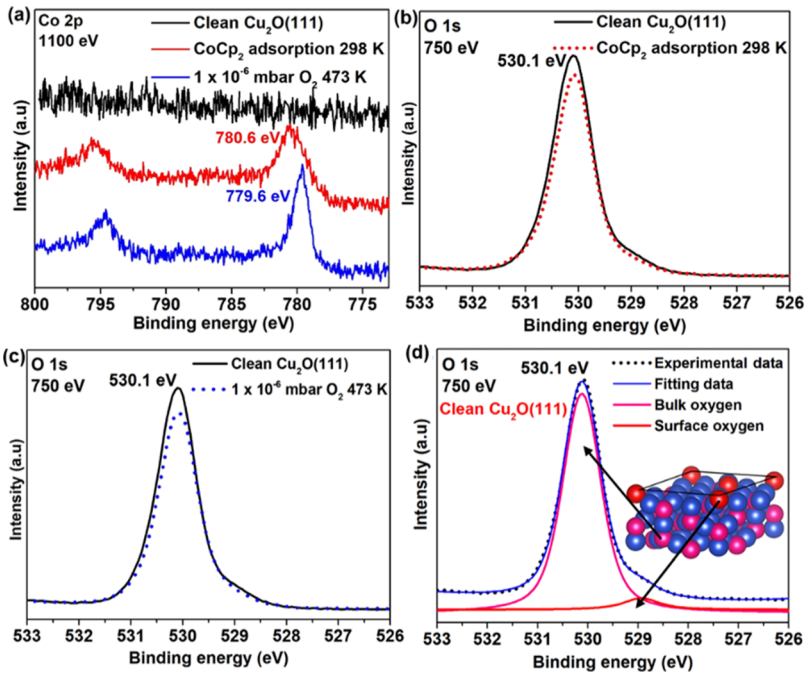
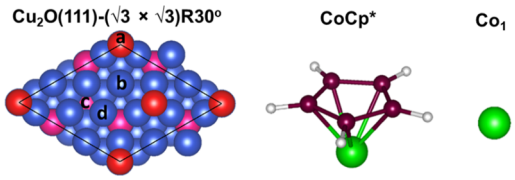


Figure 2. (a–c) Co 2p and O 1s XP spectra from a clean $Cu_2O(111)$ surface (black), after $CoCp_2$ adsorption at 298 K (red), and after annealing in 1×10^{-6} mbar O_2 at 473 K (blue). The Co coverage was 0.29 ML. The spectra were collected using photon energies of 1100 eV (Co 2p) and 750 eV (O 1s). (d) Two-component curve fit of the O 1s from the clean $Cu_2O(111)$ surface, where the red component represents oxygen atoms at surface and the pink component represents subsurface positions.

vicinity of the oxygen vacancy (Table 1). The electronic CoCp* adsorption energies (Table 1) were determined as (a) −1.69, (b) −2.78, (c) −2.79, and (d) −2.91 eV. Simulated adsorbate structures, after relaxation, are shown in Table S1. The simulations show that surface oxygen sites (a sites) are not favorable for CoCp* adsorption, in line with experimental results (STM and XPS). Adsorption of CoCp* at (b), (c), and (d) sites will after relaxation result in similar adsorption positions (see Table S1) with CoCp* residing close to the oxygen vacancy (c site). The relatively large adsorption energies of CoCp* indicate a strong interaction between the cobalt species and the surface copper atoms of $Cu_2O(111)$. The corresponding adsorption energies of Co_1, after relaxation, at the same positions as CoCp* are −1.45, −2.21, −2.39, and −2.85 eV (Table 1). Co_1 adsorbed at b and d sites will after relaxation end up at positions near the c site, similar to what was found for CoCp*. Adsorption configurations are shown in Table S1. These results are in line with observations from STM, where cobalt-containing protrusions are observed near the oxygen vacancy sites. In its most favorable adsorption geometry, Co coordinates to five copper atoms (Table S1). The combined results from the DFT simulations, STM, and XPS show that metallic single-atoms Co can be selectively deposited at positions close to the oxygen vacancy site on the $Cu_2O(111)$ surface.

Table 1. Simulated Adsorption Sites and Electronic Adsorption Energies of CoCp* and Co_1 Species on the Reconstructed $Cu_2O(111)$-$(\sqrt{3} \times \sqrt{3})R30°$ Surface[a]



initial adsorption sites	CoCp* adsorption energy (eV)	Co_1 adsorption energy (eV)
a, surface oxygen	−1.69	−1.45
b, surface copper	−2.78	−2.21
c, oxygen vacancy	−2.79	−2.39
d, surface copper	−2.91	−2.85

[a]The surface unit cell is indicated by the black rhombus. Four initial adsorption sites for CoCp* and Co_1 are marked as a, b, c, and d. Adsorption of CoCp* and Co_1 species at b and d sites results in migration to positions close to the c site after relaxation.

To further our understanding of the underlying mechanism for the selective adsorption process, we simulated the DOS using the hybrid HF-DFT PBE0 functional. Figure 3a,b shows that the valence electrons for the clean reconstructed $Cu_2O(111)$-$(\sqrt{3} \times \sqrt{3})R30°$ surface exhibit symmetrical densities for spin-up and spin-down components. The charge density is higher around the oxygen vacancy sites (Figure 3c), providing yet another indication that sites close to the oxygen vacancy are favorable for deposition of CoCp* species. Formation of a Co_1Cu HSAC at the vacancy site results in formation of a hybridized state between Cu 3d, O 2p, and Co 3d near the Fermi level (see Figure 3d–f). The perturbation of the electronic structure is a sign of a strong electronic metal–support interaction between Co_1 and Cu_2O, in line with what has been reported for other single-atom catalysis systems.[66,67] The participation of magnetic Co renders the state at the Fermi level spin-polarized. The involvement of O 2p in the hybridization is mediated through Cu since cobalt and oxygen are not in direct contact.

The reduction of surface Cu^+ on clean and Co_1Cu HSAC-modified $Cu_2O(111)$ surfaces were evaluated through exposure to a pure CO gas stream at increasing temperature and pressure. The development in the Cu chemical state was

https://doi.org/10.1021/acs.chemmater.1c04137
Chem. Mater. 2022, 34, 2313−2320

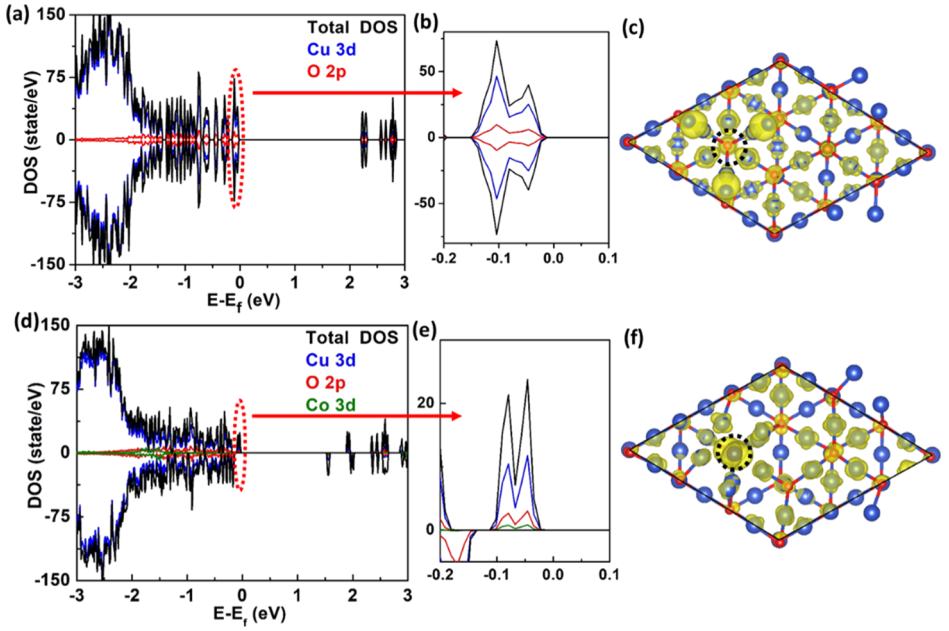


Figure 3. Simulated density of states and partial charge density distribution near the Fermi level for (a–c) clean $(\sqrt{3} \times \sqrt{3})$R30° reconstructed $Cu_2O(111)$ surface and (d–f) same surface with a single cobalt atom adsorbed near the oxygen vacancy (for adsorption geometry, see Table S1d). Iso-surface 0.0015 e/Bohr.[3] The black dashed circles in the atomic models indicate the oxygen vacancy sites. The blue and red balls represent copper and oxygen atoms, respectively.

followed by APXPS through collection of the Cu LMM Auger line. Additional experimental details and data analysis are provided in the Supporting Information, Figure S6. Figure 4a shows that the formation of metallic Cu on the clean $Cu_2O(111)$-$(\sqrt{3} \times \sqrt{3})$R30° surface proceeds slowly at 375 K in 0.32 mbar CO. This is in contrast to Cu_2O thin films grown on Cu(111) where reduction of Cu^+ is facile already at 300 K and 0.013 mbar.[11] The reduction rate significantly increases after a slight increase in temperature to 400 K (red curve). Since no molecular O_2 was supplied in the reaction follows that CO oxidation over the $Cu_2O(111)$ catalyst occurs through a Mars-van Krevelen mechanism. The reduction rate of Cu_2O is even faster at 425 K in 0.32 mbar CO gas (pink curve). At the end of the experiment, the Cu_2O surface was fully reduced, resulting in complete loss of the active Cu^+ centers. The activation energy for the CO oxidation reaction over clean $Cu_2O(111)$ was estimated to be 1.09 ± 0.10 eV (Figure S7). A drastic decrease in the reduction rate was observed when the CO gas pressure was lowered to 0.07 mbar, while the sample was kept at an even higher temperature of 415 K (not shown). These results suggest that both the reaction temperature and CO pressure are critical factors to the reduction of Cu^+ sites. For $Cu_2O(111)$ modified with 0.29 ML single-atom cobalt (Figure 4a, green curve), the Cu_2O surface remained stable throughout the experiment even as the temperature was kept at 425 K and the CO pressure increased to 1.8 mbar. The chemical state of Co also remains stable as detected by XPS (Figure S8).

Further insights on the origin of the increased stability of the $Cu_2O(111)$ surface through the modification by Co_1Cu HSAC centers at oxygen vacancy sites can be obtained from DFT calculations. Figure 4b shows that the simulated activation barrier for the abstraction of one oxygen atom by CO* from the clean reconstructed $Cu_2O(111)$-$(\sqrt{3} \times \sqrt{3})$R30° surface is 1.11 eV, in close agreement with the experimental results. After modification of the surface via Co_1Cu alloying, the

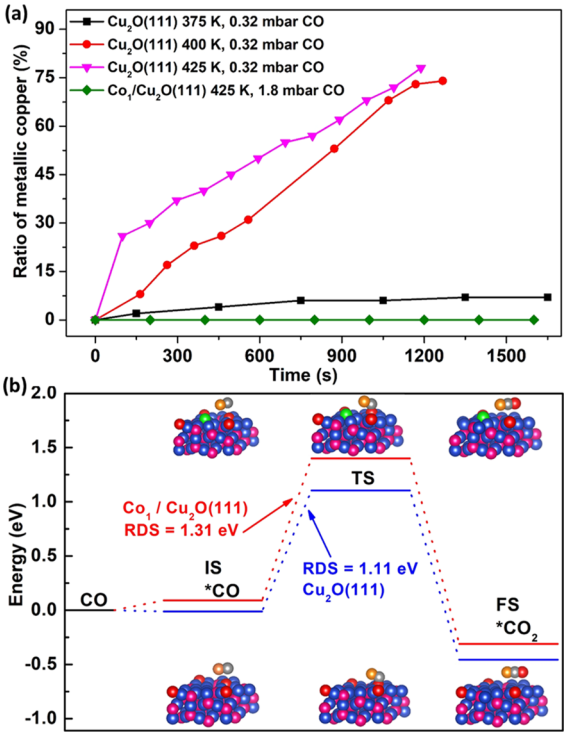


Figure 4. (a) Reduction of clean and Co_1-modified (0.29 ML) $Cu_2O(111)$ surfaces under CO conditions. The chemical state of Cu was followed in-situ by Cu LMM APXPS. (b) Potential energy surface for the simulated reaction pathways for Cu_2O reduction by CO over the clean and the Co_1Cu hybrid single-atom catalyst-modified $Cu_2O(111)$ surfaces (at site d), respectively. The atomic models depict the structures of the initial intermediate state (IS), the TS, and the final state (FS). RDS indicates the rate-determining step. Color codes: copper (blue), oxygen atoms at sub surface positions (pink), surface oxygen atoms (red), cobalt (green), CO carbon atoms (gray), and CO oxygen atoms (beige).

https://doi.org/10.1021/acs.chemmater.1c04137
Chem. Mater. 2022, 34, 2313−2320

calculated barrier increases to 1.31 eV offering a direct rationalization of the increased reduction resistance of the surface.

To summarize, the selective growth at specific sites as well as the steric hindrance of precursors demonstrates the significant strengths of the ALD method for precise synthesis of model catalysts. To the best of our knowledge, the strategy to use another metal to stabilize the active Cu^+ centers in the model catalyst has only been realized for the thin film $Cu_2O(111)$/$Cu(111)$ system through deposition of Ti using traditional PVD methods.[68] In the present paper, we investigate the modification of a single crystal surface of bulk $Cu_2O(111)$, a surface that arguably is closer to commercial powder catalyst than a thin-film system, by a selective ALD strategy more suitable for commercial applications than PVD. The deposition of isolated cobalt atoms occurs at surface vacancy sites, which allows protection of the Cu_2O surface at minimal occupancy. Co_1-stabilization of Cu_2O surfaces provides a strategy to stabilize the active Cu^+ center in Cu-based catalysts. It is also interesting to note that a Co_1Cu single-atom alloy is successfully grown on a metal oxide $Cu_2O(111)$ crystal without direct Co−O coordination. The system extends the traditional definition of single-atom alloy systems, as proposed by Sykes et al.,[27] where a metal surface serves as the support.

CONCLUSIONS

A Co_1Cu hybrid single-atom catalyst was synthesized on Cu_2O using a novel ALD strategy to address the problem of deactivation relevant to Cu_2O catalysts. The isolated Co_1Cu HSAC was grown on a reconstructed $Cu_2O(111)$-$(\sqrt{3} \times \sqrt{3})R30°$ surface at Co coverages of 0.059 and 0.29 ML. A combination of APXPS and DFT determined Co to be in a metallic state. The surface oxygen vacancies of the $Cu_2O(111)$-$(\sqrt{3} \times \sqrt{3})R30°$ reconstructed surface are the most favorable adsorption sites for the single-atom Co species and results in the formation of a hybrid spin polarized state close to the Fermi level. The reduction of surface Cu, under CO conditions, was evaluated for both the clean $Cu_2O(111)$ surface and for surfaces modified by Co_1Cu hybrid SAAs through collection of ambient-pressure Auger Cu LMM spectra. The experimental reduction barrier over the clean $Cu_2O(111)$-$(\sqrt{3} \times \sqrt{3})R30°$ surface is close to the DFT-obtained reaction barrier. According to the DFT simulations, cobalt stabilizes the Cu_2O surface by increasing the activation barrier of surface oxygen abstraction. APXPS confirmed the stability of the modified surface under reaction conditions. The presented methods and results provide new experimental and theoretical insights that may be extended to address problems of deactivation persistent in Cu-based catalysts. The new type of Co_1Cu HSAC obtained on a Cu_2O metal-oxide support may provide a way to bridge SAA catalysts and oxide-supported SACs.

ASSOCIATED CONTENT

Supporting Information

The Supporting Information is available free of charge at https://pubs.acs.org/doi/10.1021/acs.chemmater.1c04137.

STM images from the clean $Cu_2O(111)$ surface and from different stages in the cobalt growth process, simulated adsorbate structures of CoCp and Co on the $Cu_2O(111)$ crystal, additional Cu LMM and Co 2p XPS spectra, and description of the fitting procedure (PDF)

AUTHOR INFORMATION

Corresponding Author

Jonas Weissenrieder − *Materials and Nano Physics, School of Engineering Sciences, KTH Royal Institute of Technology, SE-100 44 Stockholm, Sweden;* orcid.org/0000-0003-1631-4293; Email: jonas@kth.se

Authors

Chunlei Wang − *Materials and Nano Physics, School of Engineering Sciences, KTH Royal Institute of Technology, SE-100 44 Stockholm, Sweden*

Yuan Kong − *Hefei National Laboratory for Physical Sciences at the Microscale & Synergetic Innovation Center of Quantum Information and Quantum Physics & CAS Center for Excellence in Nanoscience and Department of Chemical Physics & Key Laboratory of Surface and Interface Chemistry and Energy Catalysis of Anhui Higher Education Institutes, University of Science and Technology of China, Hefei 230026 Anhui, China*

Markus Soldemo − *Materials and Nano Physics, School of Engineering Sciences, KTH Royal Institute of Technology, SE-100 44 Stockholm, Sweden*

Zongfang Wu − *Materials and Nano Physics, School of Engineering Sciences, KTH Royal Institute of Technology, SE-100 44 Stockholm, Sweden*

Héloise Tissot − *CINaM, UMR 7325, Aix-Marseille Univ., CNRS, F-13288 Marseille, France*

Burcu Karagoz − *Center for Functional Nanomaterials, Brookhaven National Laboratory, Upton 11973 New York, United States*

Kess Marks − *Materials and Nano Physics, School of Engineering Sciences, KTH Royal Institute of Technology, SE-100 44 Stockholm, Sweden*

Joakim Halldin Stenlid − *SUNCAT Center for Interface Science and Catalysis, SLAC National Accelerator Laboratory, Menlo Park 94025 California, United States; Department of Chemical Engineering, Stanford University, Stanford 94305 California, United States;* orcid.org/0000-0003-3832-2331

Andrey Shavorskiy − *MAX IV Laboratory, Lund University, 221 00 Lund, Sweden;* orcid.org/0000-0002-7517-5089

Esko Kokkonen − *MAX IV Laboratory, Lund University, 221 00 Lund, Sweden;* orcid.org/0000-0002-3674-7486

Sarp Kaya − *Koç University Tüpraş Energy Center (KUTEM), Department of Chemistry, Koç University, 34450 Istanbul, Turkey;* orcid.org/0000-0002-2591-5843

Dario J. Stacchiola − *Center for Functional Nanomaterials, Brookhaven National Laboratory, Upton 11973 New York, United States;* orcid.org/0000-0001-5494-3205

Complete contact information is available at: https://pubs.acs.org/10.1021/acs.chemmater.1c04137

Author Contributions

○C.W., Y.K. contributed equally to this work.

Notes

The authors declare no competing financial interest.

ACKNOWLEDGMENTS

This work was funded by the Ministry of Science and Technology of China (no. 2017YFA0204904), the Swedish Research Council (VR), the Knut och Alice Wallenbergs stiftelse, and STINT Joint China-Sweden Mobility program.

H.T. acknowledges the financial support from the Ragnar Holm foundation, and C.W. acknowledges the financial support from Trygger's foundation. The computational resources were provided by the supercomputing system in the Supercomputing Center of University of Science and Technology of China. The MAX IV staff is gratefully acknowledged for their support on beamlines HIPPIE and SPECIES. Research conducted at MAX IV, a Swedish national user facility, is supported by the Swedish Research Council under contract 2018-07152, the Swedish Governmental Agency for Innovation Systems under contract 2018-04969, and Formas under contract 2019-02496. S.K. thanks TARLA for collaborative research effort.

REFERENCES

(1) Royer, S.; Duprez, D. Catalytic Oxidation of Carbon Monoxide over Transition Metal Oxides. *Chemcatchem* **2011**, *3*, 24−65.
(2) Gao, Y.; Zhang, L.; van Hoof, A. J. F.; Hensen, E. J. M. On the surface-dependent oxidation of Cu_2O during CO oxidation: Cu^{2+} is more active than Cu^{+}. *Appl. Catal., A* **2020**, *602*, 117712.
(3) Tsai, M.-L.; Hadt, R. G.; Vanelderen, P.; Sels, B. F.; Schoonheydt, R. A.; Solomon, E. I. $[Cu_2O]^{2+}$ active site formation in Cu−ZSM-5: geometric and electronic structure requirements for N_2O activation. *J. Am. Chem. Soc.* **2014**, *136*, 3522−3529.
(4) Schulz, K. H.; Cox, D. F. Propene Oxidation over Cu_2O Single-Crystal Surfaces - a Surface Science Study of Propene Activation at 1 Atm and 300 K. *J. Catal.* **1993**, *143*, 464−480.
(5) Hua, Q.; Cao, T.; Gu, X.-K.; Lu, J.; Jiang, Z.; Pan, X.; Luo, L.; Li, W.-X.; Huang, W. Crystal-Plane-Controlled selectivity of Cu_2O catalysts in propylene oxidation with molecular oxygen. *Angew. Chem.* **2014**, *126*, 4956−4961.
(6) Zhang, Z.; Wang, S.-S.; Song, R.; Cao, T.; Luo, L.; Chen, X.; Gao, Y.; Lu, J.; Li, W.-X.; Huang, W. The most active Cu facet for low-temperature water gas shift reaction. *Nat. Commun.* **2017**, *8*, 488.
(7) Paracchino, A.; Laporte, V.; Sivula, K.; Grätzel, M.; Thimsen, E. Highly active oxide photocathode for photoelectrochemical water reduction. *Nat. Mater.* **2011**, *10*, 456−461.
(8) Liu, Z.; Huang, E.; Orozco, I.; Liao, W.; Palomino, R. M.; Rui, N.; Duchoň, T.; Nemšák, S.; Grinter, D. C.; Mahapatra, M.; Liu, P.; Rodriguez, J. A.; Senanayake, S. D. Water-promoted interfacial pathways in methane oxidation to methanol on a CeO_2-Cu_2O catalyst. *Science* **2020**, *368*, 513−517.
(9) Hagman, B.; Posada-Borbón, A.; Schaefer, A.; Shipilin, M.; Zhang, C.; Merte, L. R.; Hellman, A.; Lundgren, E.; Grönbeck, H.; Gustafson, J. Steps control the dissociation of CO_2 on Cu (100). *J. Am. Chem. Soc.* **2018**, *140*, 12974−12979.
(10) Xu, F.; Mudiyanselage, K.; Baber, A. E.; Soldemo, M.; Weissenrieder, J.; White, M. G.; Stacchiola, D. J. Redox-mediated reconstruction of copper during carbon monoxide oxidation. *J. Phys. Chem. C* **2014**, *118*, 15902−15909.
(11) Baber, A. E.; Xu, F.; Dvorak, F.; Mudiyanselage, K.; Soldemo, M.; Weissenrieder, J.; Senanayake, S. D.; Sadowski, J. T.; Rodriguez, J. A.; Matolín, V.; White, M. G.; Stacchiola, D. J. In Situ Imaging of Cu_2O under Reducing Conditions: Formation of Metallic Fronts by Mass Transfer. *J. Am. Chem. Soc.* **2013**, *135*, 16781−16784.
(12) Jernigan, G. G.; Somorjai, G. A. Carbon monoxide oxidation over three different oxidation states of copper: metallic copper, copper (I) oxide, and copper (II) oxide-a surface science and kinetic study. *J. Catal.* **1994**, *147*, 567−577.
(13) Huang, T.-J.; Tsai, D.-H. CO oxidation behavior of copper and copper oxides. *Catal. Lett.* **2003**, *87*, 173−178.
(14) Bao, H.; Zhang, W.; Hua, Q.; Jiang, Z.; Yang, J.; Huang, W. Crystal-Plane-Controlled Surface Restructuring and Catalytic Performance of Oxide Nanocrystals. *Angew. Chem.* **2011**, *123*, 12502−12506.
(15) Yu, J.; Yang, M.; Zhang, J.; Ge, Q.; Zimina, A.; Pruessmann, T.; Zheng, L.; Grunwaldt, J.-D.; Sun, J. Stabilizing Cu^{+} in Cu/SiO2 Catalysts with a Shattuckite-Like Structure Boosts CO_2 Hydrogenation into Methanol. *ACS Catal.* **2020**, *10*, 14694−14706.
(16) Liu, L.; Corma, A. Metal catalysts for heterogeneous catalysis: from single atoms to nanoclusters and nanoparticles. *Chem. Rev.* **2018**, *118*, 4981−5079.
(17) Qiao, B.; Wang, A.; Yang, X.; Allard, L. F.; Jiang, Z.; Cui, Y.; Liu, J.; Li, J.; Zhang, T. Single-atom catalysis of CO oxidation using Pt_1/FeO_x. *Nat. Chem.* **2011**, *3*, 634−641.
(18) Wang, A.; Li, J.; Zhang, T. Heterogeneous single-atom catalysis. *Nat. Rev. Chem.* **2018**, *2*, 65−81.
(19) Ding, K.; Gulec, A.; Johnson, A. M.; Schweitzer, N. M.; Stucky, G. D.; Marks, L. D.; Stair, P. C. Identification of active sites in CO oxidation and water-gas shift over supported Pt catalysts. *Science* **2015**, *350*, 189−192.
(20) Hannagan, R. T.; Giannakakis, G.; Flytzani-Stephanopoulos, M.; Sykes, E. C. H. Single-atom alloy catalysis. *Chem. Rev.* **2020**, *120*, 12044−12088.
(21) Hulva, J.; Meier, M.; Bliem, R.; Jakub, Z.; Kraushofer, F.; Schmid, M.; Diebold, U.; Franchini, C.; Parkinson, G. S. Unraveling CO adsorption on model single-atom catalysts. *Science* **2021**, *371*, 375−379.
(22) Zhou, X.; Shen, Q.; Yuan, K.; Yang, W.; Chen, Q.; Geng, Z.; Zhang, J.; Shao, X.; Chen, W.; Xu, G.; Yang, x.; Wu, K. Unraveling charge state of supported Au single-atoms during CO oxidation. *J. Am. Chem. Soc.* **2018**, *140*, 554−557.
(23) Dvořák, F.; Camellone, M. F.; Tovt, A.; Tran, N.-D.; Negreiros, F. R.; Vorokhta, M.; Skála, T.; Matolínová, I.; Mysliveček, J.; Matolín, V. Creating single-atom Pt-ceria catalysts by surface step decoration. *Nat. Commun.* **2016**, *7*, 10801.
(24) Parkinson, G. S. Unravelling single atom catalysis: The surface science approach. *Chin. J. Catal.* **2017**, *38*, 1454−1459.
(25) Kyriakou, G.; Boucher, M. B.; Jewell, A. D.; Lewis, E. A.; Lawton, T. J.; Baber, A. E.; Tierney, H. L.; Flytzani-Stephanopoulos, M.; Sykes, E. C. H. Isolated metal atom geometries as a strategy for selective heterogeneous hydrogenations. *Science* **2012**, *335*, 1209−1212.
(26) Hannagan, R. T.; Giannakakis, G.; Réocreux, R.; Schumann, J.; Finzel, J.; Wang, Y.; Michaelides, A.; Deshlahra, P.; Christopher, P.; Flytzani-Stephanopoulos, M.; Stamatakis, M.; Sykes, E. C. H. First-principles design of a single-atom−alloy propane dehydrogenation catalyst. *Science* **2021**, *372*, 1444−1447.
(27) Giannakakis, G.; Flytzani-Stephanopoulos, M.; Sykes, E. C. H. Single-atom alloys as a reductionist approach to the rational design of heterogeneous catalysts. *Acc. Chem. Res.* **2018**, *52*, 237−247.
(28) Mao, J.; Yin, J.; Pei, J.; Wang, D.; Li, Y. Single atom alloy: An emerging atomic site material for catalytic applications. *Nano Today* **2020**, *34*, 100917.
(29) Marcinkowski, M. D.; Darby, M. T.; Liu, J.; Wimble, J. M.; Lucci, F. R.; Lee, S.; Michaelides, A.; Flytzani-Stephanopoulos, M.; Stamatakis, M.; Sykes, E. C. H. Pt/Cu single-atom alloys as coke-resistant catalysts for efficient C−H activation. *Nat. Chem.* **2018**, *10*, 325−332.
(30) Greiner, M. T.; Jones, T. E.; Beeg, S.; Zwiener, L.; Scherzer, M.; Girgsdies, F.; Piccinin, S.; Armbrüster, M.; Knop-Gericke, A.; Schlögl, R. Free-atom-like d states in single-atom alloy catalysts. *Nat. Chem.* **2018**, *10*, 1008−1015.
(31) Kruppe, C. M.; Krooswyk, J. D.; Trenary, M. Selective hydrogenation of acetylene to ethylene in the presence of a carbonaceous surface layer on a Pd/Cu(111) single-atom alloy. *ACS Catal.* **2017**, *7*, 8042−8049.
(32) Cao, L.; Lu, J. Atomic-scale engineering of metal−oxide interfaces for advanced catalysis using atomic layer deposition. *Catal. Sci. Technol.* **2020**, *10*, 2695−2710.
(33) Zhu, S.; Scardamaglia, M.; Kundsen, J.; Sankari, R.; Tarawneh, H.; Temperton, R.; Pickworth, L.; Cavalca, F.; Wang, C.; Tissot, H.; Weissenrieder, J.; Hagman, B.; Gustafson, J.; Kaya, S.; Lindgren, F.; Källquist, I.; Maibach, J.; Hahlin, M.; Boix, V.; Gallo, T.; Rehman, F.; D'Acunto, G.; Schnadt, J.; Shavorskiy, A. HIPPIE: a new platform for

ambient-pressure X-ray photoelectron spectroscopy at the MAX IV Laboratory. *J. Synchrotron Radiat.* **2021**, *28*, 624−636.
(34) Urpelainen, S.; Såthe, C.; Grizolli, W.; Agåker, M.; Head, A. R.; Andersson, M.; Huang, S.-W.; Jensen, B. N.; Wallén, E.; Tarawneh, H.; Sankari, R.; Nyholm, R.; Lindberg, M.; Sjöblom, P.; Johansson, N.; Reinecke, B. N.; Arman, M. A.; Merte, L. R.; Knudsen, J.; Schnadt, J.; Andersen, J. N.; Hennies, F. The SPECIES beamline at the MAX IV Laboratory: a facility for soft X-ray RIXS and APXPS. *J. Synchrotron Radiat.* **2017**, *24*, 344−353.
(35) Kokkonen, E.; Lopes da Silva, F.; Mikkelã, M.-H.; Johansson, N.; Huang, S.-W.; Lee, J.-M.; Andersson, M.; Bartalesi, A.; Reinecke, B. N.; Handrup, K.; Tarawneh, H.; Sankari, R.; Knudsen, J.; Schnadt, J.; Såthe, C.; Urpelainen, S. Upgrade of the SPECIES beamline at the MAX IV Laboratory. *J. Synchrotron Radiat.* **2021**, *28*, 588−601.
(36) Hohenberg, P.; Kohn, W. Inhomogeneous electron gas. *Phys. Rev.* **1964**, *136*, B864.
(37) Kohn, W.; Sham, L. J. Self-consistent equations including exchange and correlation effects. *Phys. Rev.* **1965**, *140*, A1133.
(38) Kresse, G.; Furthmüller, J. Software VASP, vienna (1999). *Phys. Rev. B: Condens. Matter Mater. Phys.* **1996**, *54*, 169.
(39) Blöchl, P. E. Projector augmented-wave method. *Phys. Rev. B: Condens. Matter Mater. Phys.* **1994**, *50*, 17953.
(40) Kresse, G.; Joubert, D. From ultrasoft pseudopotentials to the projector augmented-wave method. *Phys. Rev. B: Condens. Matter Mater. Phys.* **1999**, *59*, 1758.
(41) Hammer, B.; Hansen, L. B.; Nørskov, J. K. Improved adsorption energetics within density-functional theory using revised Perdew-Burke-Ernzerhof functionals. *Phys. Rev. B: Condens. Matter Mater. Phys.* **1999**, *59*, 7413.
(42) Önsten, A.; Göthelid, M.; Karlsson, U. O. Atomic structure of Cu_2O(111). *Surf. Sci.* **2009**, *603*, 257−264.
(43) Li, C.; Wang, F.; Li, S. F.; Sun, Q.; Jia, Y. Stability and electronic properties of the O-terminated Cu_2O(111) surfaces: First-principles investigation. *Phys. Lett. A* **2010**, *374*, 2994−2998.
(44) Sun, B.-Z.; Chen, W.-K.; Zheng, J.-D.; Lu, C.-H. Roles of oxygen vacancy in the adsorption properties of CO and NO on Cu_2O(111) surface: Results of a first-principles study. *Appl. Surf. Sci.* **2008**, *255*, 3141−3148.
(45) Tissot, H.; Wang, C.; Stenlid, J. H.; Panahi, M.; Kaya, S.; Soldemo, M.; Ghadami Yazdi, M.; Brinck, T.; Weissenrieder, J. Interaction of Atomic Hydrogen with the Cu_2O(100) and (111) Surfaces. *J. Phys. Chem. C* **2019**, *123*, 22172−22180.
(46) Henkelman, G.; Uberuaga, B. P.; Jónsson, H. A climbing image nudged elastic band method for finding saddle points and minimum energy paths. *J. Chem. Phys.* **2000**, *113*, 9901−9904.
(47) Adamo, C.; Barone, V. Toward reliable density functional methods without adjustable parameters: The PBE0 model. *J. Chem. Phys.* **1999**, *110*, 6158−6170.
(48) Yan, H.; Zhao, X.; Guo, N.; Lyu, Z.; Du, Y.; Xi, S.; Guo, R.; Chen, C.; Chen, Z.; Liu, W.; Yao, C.; Li, J.; Pennycook, S. J.; Chen, W.; Su, C.; Zhang, C.; Lu, J. Atomic engineering of high-density isolated Co atoms on graphene with proximal-atom controlled reaction selectivity. *Nat. Commun.* **2018**, *9*, 3197.
(49) Cao, L.; Liu, W.; Luo, Q.; Yin, R.; Wang, B.; Weissenrieder, J.; Soldemo, M.; Yan, H.; Lin, Y.; Sun, Z.; Ma, C.; Zhang, W.; Chen, S.; Wang, H.; Guan, Q.; Yao, T.; Wei, S.; Yang, J.; Lu, J. Atomically dispersed iron hydroxide anchored on Pt for preferential oxidation of CO in H_2. *Nature* **2019**, *565*, 631−635.
(50) Önsten, A.; Weissenrieder, J.; Stoltz, D.; Yu, S.; Göthelid, M.; Karlsson, U. O. Role of defects in surface chemistry on Cu_2O (111). *J. Phys. Chem. C* **2013**, *117*, 19357−19364.
(51) Wang, C.; Tissot, H.; Escudero, C.; Pérez-Dieste, V.; Stacchiola, D.; Weissenrieder, J. Redox Properties of Cu_2O(100) and (111) Surfaces. *J. Phys. Chem. C* **2018**, *122*, 28684−28691.
(52) Barber, M.; Connor, J. A.; Derrick, L. M. R.; Hall, M. B.; Hillier, I. H. High energy photoelectron spectroscopy of transition metal complexes. Part 2—Metallocenes. *J. Chem. Soc., Faraday Trans. 2* **1973**, *69*, 559−562.
(53) O'Hare, D.; Jaegermann, W.; Williamson, D. L.; Ohuchi, F. S.; Parkinson, B. A. X-ray photoelectron, Moessbauer, magnetic and electrical conductivity study of SnS_2 $\{CoCp_2\}$ 0.31. *Inorg. Chem.* **1988**, *27*, 1537−1542.
(54) Brundle, C. R.; Chuang, T. J.; Rice, D. W. X-ray photoemission study of the interaction of oxygen and air with clean cobalt surfaces. *Surf. Sci.* **1976**, *60*, 286−300.
(55) Bazylewski, P.; Boukhvalov, D. W.; Kukharenko, A. I.; Kurmaev, E. Z.; Hunt, A.; Moewes, A.; Lee, Y. H.; Cholakh, S. O.; Chang, G. S. The characterization of Co-nanoparticles supported on graphene. *RSC Adv.* **2015**, *5*, 75600−75606.
(56) Shen, Z.-X.; Allen, J. W.; Lindberg, P. A. P.; Dessau, D. S.; Wells, B. O.; Borg, A.; Ellis, W.; Kang, J. S.; Oh, S.-J.; Lindau, I.; Spicer, W. E. Photoemission study of CoO. *Phys. Rev. B: Condens. Matter Mater. Phys.* **1990**, *42*, 1817.
(57) Frost, D. C.; McDowell, C. A.; Woolsey, I. S. X-ray photoelectron spectra of cobalt compounds. *Mol. Phys.* **1974**, *27*, 1473−1489.
(58) Chuang, T. J.; Brundle, C. R.; Rice, D. W. Interpretation of the x-ray photoemission spectra of cobalt oxides and cobalt oxide surfaces. *Surf. Sci.* **1976**, *59*, 413−429.
(59) Zhong, L.; Kropp, T.; Baaziz, W.; Ersen, O.; Teschner, D.; Schlögl, R.; Mavrikakis, M.; Zafeiratos, S. Correlation Between Reactivity and Oxidation State of Cobalt Oxide Catalysts for CO Preferential Oxidation. *ACS Catal.* **2019**, *9*, 8325−8336.
(60) Dai, E.; Xu, J.; Qiu, J.; Liu, S.; Chen, P.; Liu, Y. Co@ Carbon and Co_3O_4@ Carbon nanocomposites derived from a single MOF for supercapacitors. *Sci. Rep.* **2017**, *7*, 12588.
(61) Kim, M.-J.; Na, H.-J.; Lee, K. C.; Yoo, E. A.; Lee, M. Preparation and characterization of Au−Ag and Au−Cu alloy nanoparticles in chloroform. *J. Mater. Chem.* **2003**, *13*, 1789−1792.
(62) Cole, R. J.; Brooks, N. J.; Weightman, P. Determination of charge transfer in the Cu_xPd_{1-x} alloy system. *Phys. Rev. B: Condens. Matter Mater. Phys.* **1997**, *56*, 12178.
(63) Kim, H.; Park, H.; Oh, S.; Kim, S. K. Facile electrochemical preparation of nonprecious Co-Cu alloy catalysts for hydrogen production in proton exchange membrane water electrolysis. *Int. J. Energy Res.* **2020**, *44*, 2833−2844.
(64) Cao, Y.; Chen, S.; Luo, Q.; Yan, H.; Lin, Y.; Liu, W.; Cao, L.; Lu, J.; Yang, J.; Yao, T.; Wei, S. Atomic-Level Insight into Optimizing the Hydrogen Evolution Pathway over a Co_1-N4 Single-Site Photocatalyst. *Angew. Chem., Int. Ed.* **2017**, *56*, 12191−12196.
(65) Wang, H.; Luo, Q.; Liu, W.; Lin, Y.; Guan, Q.; Zheng, X.; Pan, H.; Zhu, J.; Sun, Z.; Wei, S.; Yang, J.; Lu, J. Quasi Pd 1 Ni single-atom surface alloy catalyst enables hydrogenation of nitriles to secondary amines. *Nat. Commun.* **2019**, *10*, 4998.
(66) Hu, P.; Huang, Z.; Amghouz, Z.; Makkee, M.; Xu, F.; Kapteijn, F.; Dikhtiarenko, A.; Chen, Y.; Gu, X.; Tang, X. Electronic metal−support interactions in single-atom catalysts. *Angew. Chem.* **2014**, *126*, 3486−3489.
(67) Yang, J.; Li, W.; Wang, D.; Li, Y. Electronic Metal−Support Interaction of Single-Atom Catalysts and Applications in Electrocatalysis. *Adv. Mater.* **2020**, *32*, 2003300.
(68) Baber, A. E.; Yang, X.; Kim, H. Y.; Mudiyanselage, K.; Soldemo, M.; Weissenrieder, J.; Senanayake, S. D.; Al-Mahboob, A.; Sadowski, J. T.; Evans, J.; Rodriguez, J. A.; Liu, P.; Hoffmann, F. M.; Chen, J. G.; Stacchiola, D. J. Stabilization of Catalytically Active Cu^+ Surface Sites on Titanium-Copper Mixed-Oxide Films. *Angew. Chem., Int. Ed.* **2014**, *126*, 5440−5444.

NOTE ADDED AFTER ASAP PUBLICATION

This paper was published ASAP on February 3, 2022, with the incorrect Supporting Information file. The corrected version was reposted on February 16, 2022.

https://doi.org/10.1021/acs.chemmater.1c04137
Chem. Mater. 2022, 34, 2313−2320